Disclinations without Gradients: A Nonlocal Model for Topological Defects in Liquid Crystals

Robert Buarque de Macedo[*], Hossein Pourmatin[†], Timothy Breitzman[‡], Kaushik Dayal[§]

[*]Department of Physics, Carnegie Mellon University

[†§]Department of Civil and Environmental Engineering, Carnegie Mellon University

[‡]Composites Branch, Air Force Research Laboratory

[§]Center for Nonlinear Analysis, Carnegie Mellon University

[§]Department of Materials Science and Engineering, Carnegie Mellon University

June 19, 2018

Abstract

Nematic liquid crystals composed of rod-like molecules have an orientational elasticity that accounts for the energetics of the molecular orientation. This elasticity can be described by a unit vector field; the unit vector constraint interacts with even fairly simple boundary conditions to cause disclination defects. Disclinations are entirely a topological consequence of the kinematic constraint, and occur irrespective of the particular energetic model. Because disclinations are topological defects, they cannot be regularized by adding higher gradients, as in phase-field models of interface defects. On the contrary, the higher gradient terms would cause even greater singularities in the energy. In this paper, we formulate an integral-based nonlocal regularized energy for nematic liquid crystals. Our model penalizes disclination cores and thereby enforces a finite width, while the integral regularization ensures that the defect core energy is bounded and finite. The regularization at the same time tends to the standard gradient-based energies away from the disclination, as well as building in the head-tail symmetry. We characterize the formulation in its ability to describe disclinations of various strengths, and then apply it to examine: (1) the stability and decomposition of various disclinations, and the competition between bend and splay energies in determining the relative stability of integer and half-integer disclinations (2) the coalescence of a $+\frac{1}{2}$ and $-\frac{1}{2}$ disclination pair; we find the disclinations do *not* move at the same velocities towards each other, suggesting that the asymmetry of the director field plays a dominant role despite the equal-and-opposite topological strengths of the disclinations.

[*]Email: rabm1993@gmail.com
[†]Email: mpourmat@andrew.cmu.edu
[‡]Email: timothy.breitzman.1@us.af.mil
[§]Email: Kaushik.Dayal@cmu.edu

1 Introduction

Nematic liquid crystals are composed of rod-like molecules that have no positional ordering but tend to align along the same direction. There is therefore an energetic penalty – an orientational elasticity – for spatial variations in the direction. In a continuum mesoscale description, the kinematics of the orientational ordering can be described by a unit vector field $\boldsymbol{n}$– the *director field* – that tracks the average ordering of the molecules. The orientational elasticity is then described by an energy that depends on $\nabla \boldsymbol{n}$ in a very nonlinear way [Ste04, KL07, CL00]. There are two key challenges associated with using $\nabla \boldsymbol{n}$. First, the director is constrained to be a unit vector field because it represents directions, i.e. $|\boldsymbol{n}| = 1$. Second, the head-tail symmetry of nonpolar liquid crystal molecules imposes the constraint that the energy is invariant under the transformation $\boldsymbol{n} \leftrightarrow -\boldsymbol{n}$.

These constraints make the model severely nonlinear. In addition, the constraints – in combination with boundary conditions – can lead to the formation of topological defects. Fig. 1 shows classical examples. The $+1$ disclination forms when the boundary conditions set the director on the boundaries. At some point in the interior, the director field must be discontinuous if it satisfies the unit constraint; in this ideal case, the disclination is at the center by symmetry. There is no way to set up the director field to be continuous everywhere with the given boundary conditions. The $+\frac{1}{2}$ disclination forms when the boundary conditions are as shown in the figure. In addition to the discontinuity at the center, the head-tail symmetry also leads to a discontinuous line (in 2D) if it is represented by a director vector field $\boldsymbol{n}$. If we assume that the vectors on the right edge all point upwards and follow the vectors anti-clockwise in the upper half and clockwise in the lower half, we find that the vectors point in opposite directions on either side of the line $(x_1 < 0, x_2 = 0)$.

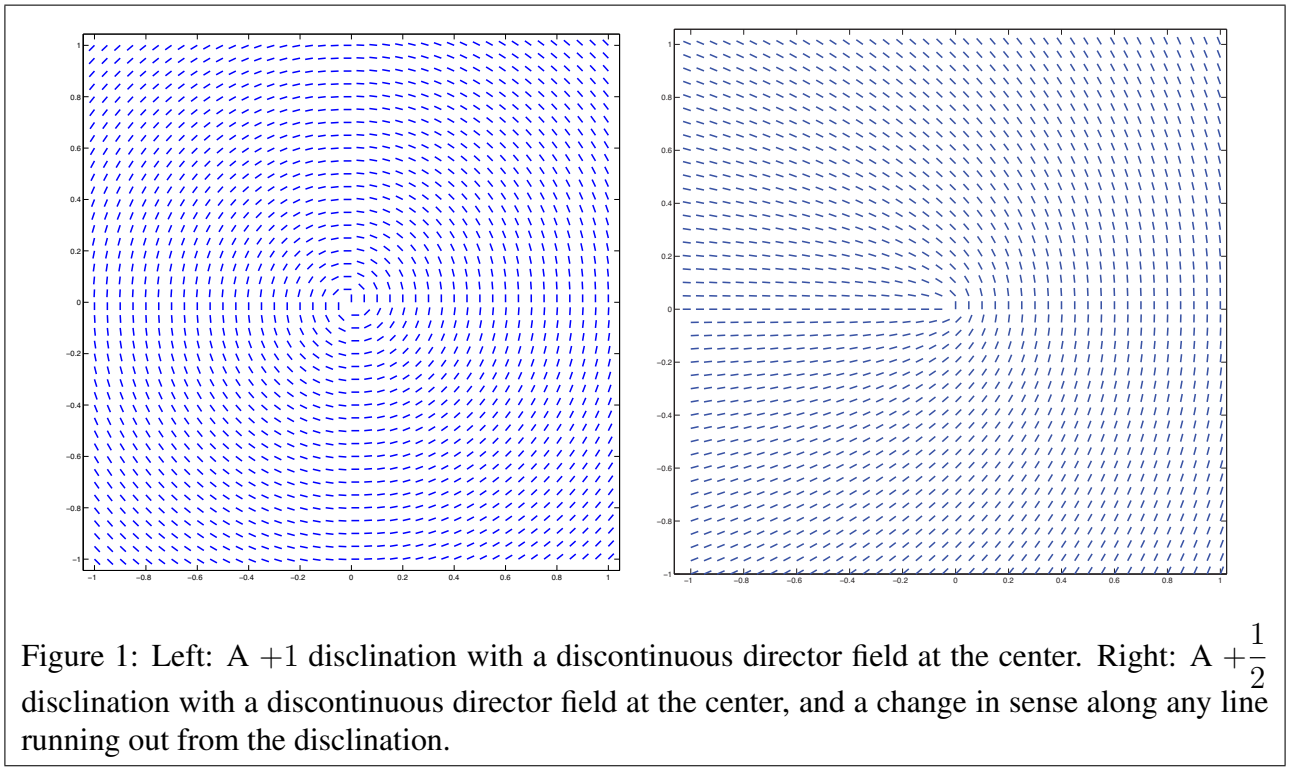

Figure 1: Left: A $+1$ disclination with a discontinuous director field at the center. Right: A $+\frac{1}{2}$ disclination with a discontinuous director field at the center, and a change in sense along any line running out from the disclination.

The topological nature of disclinations and their connection to boundary conditions is in contrast to in-

terfaces, cracks, and other defects that are not topological. In the latter, boundary conditions certainly play an important role, but through the energy rather than geometry; i.e., whether a defect forms or not depends on the energetics of the particular model. An important consequence of this distinction is that phase-field models are readily constructed for the latter class of defects, because adding gradient contributions to the energy (accounting for surface energies) smooths out the discontinuities. In contrast, there is no such simple approach for disclinations which are driven by the boundary. Adding gradient contributions to the energy cannot smooth out the defect; on the contrary, the presence of higher derivatives makes the energy more singular at a disclination.

A proposed approach for disclinations is by Ericksen [Eri91], in which he introduces a new scalar order parameter in addition to the director field. The scalar order parameter is used to track the disclination cores and evolves using a separate equation. Another approach in this spirit of introducing another field to track defects is [AD14, PAD15], where a tensor order parameter is introduced, and a geometrically-motivated evolution equation is posed. In contrast to these, we regularize the energy, but do not introduce a new field variable nor an associated evolution equation.

The most widely-applied regularized model that is used to model disclinations is the Q-tensor model [MN14]. Briefly, the order parameter is a tensor $\boldsymbol{Q}$ that is related to the tensor dyad $\boldsymbol{n} \otimes \boldsymbol{n}$[1] away from a defect, and at a defect the material is no longer uniaxial and cannot be described by a single director. At the defect core, the eigenvectors of $\boldsymbol{Q}$ aim to capture some key information about the orientational distribution function [MN14]. Core effects are introduced by energetic contributions in terms of the gradients of $\boldsymbol{Q}$. Q-tensor models, however, also make certain predictions that are significantly at odds with the director-based models. In the static setting, consider 2 infinite parallel plates with tangential anchoring and normal anchoring on the top and bottom respectively. As observed by [PMGK94], there are regimes in which the Q-tensor model predicts a loss of uniaxiality throughout the domain, i.e., the entire domain is defect-like. In contrast, the simple 1-constant director-based model has a solution with a linear variation of the angle from top to bottom. Similarly contrasting predictions are observed with the Q-tensor model in various geometries and boundary conditions, e.g. [BGJRV03, CLB$^+$09, BVD04]. In the dynamic setting, Ericksen and Leslie provided a physical model based on conservation laws – mass, linear momentum, and angular momentum – for the evolution of the director [Ste04]. In contrast, the evolution principles for $\boldsymbol{Q}$ in the Q-tensor model are typically based on non-equilibrium thermodynamics, for instance either (1) a Rayleigh dissipation principle, e.g. [SMV04], or (2) ideas from kinetic theory, e.g. [KLGCC08, YFMW09], but the issue of the closure assumption for the moments of the orientation distribution function is a further assumption. In our view, these evolution principles for $\boldsymbol{Q}$ are not as fundamental as the principle of angular momentum balance.

The issues above motivate the current work. We propose a nonlocal (integral) regularization of the energy that accounts for core effects in a natural way, yet retains the many attractive features of a director field based model. First, the regularization introduces a length scale that enables us to describe disclinations with a finite width; second, using integrals rather than derivatives enables us to have disclinations of finite energy even when the director field is topologically constrained to be singular; third, we do not need to relax the unit vector constraint as some other models require; and finally, retaining the director field description enables the use of angular momentum principles to prescribe the evolution.

We note that it is particularly important not to relax the unit vector constraint; it is based on the direction corresponding to the orientation of the molecules, and hence relaxing the constraint to allow for non-unit vectors is not physically meaningful. Therefore, a regularization based on relaxing the unit-vector

[1] This ensures the head-tail symmetry is captured.

constraint is not particularly physical, even if it is computationally convenient.

We emphasize 3 important features of the proposed integral regularization of the energy:

- For homogeneous – i.e. linearly varying – director fields, we should recover the classical energy;
- Only a constant director field must have zero energy; any other spatial variation of the director field must cost energy;
- It should not require continuity of the field

The first requirement ensures that we recover the standard Ericksen-Leslie model when we are far from disclinations or in disclination-free configurations. The second requirement ensures that our solutions are not "polluted" by unphysical zero-energy soft modes; except for rigid motions, the energy must increase when deformed. The third requirement ensures that disclinations can be modeled.

Our integral model is motivated largely by the peridynamic model of fracture, in which integral operators are used to approximate standard elasticity operators, thereby allowing fields to be discontinuous as is essential for fracture [Sil00, SL10].

We have ignored the coupling to fluid flow in this work. It is conceptually straightforward to replace the classical energy by our regularized energy to construct a model with director evolution coupled to flow.

1.1 Organization

The paper is organized as follows.

- In Section 2, we briefly outline the key features of the energetics of the classical model of liquid crystals. This is primarily to show the analogies and contrasts with our proposed model.
- In Section 3, we describe the proposed nonlocal regularized energy without gradients. Specifically, we (1) motivate the connection between integral operators and gradient operators, (2) formulate the nonlocal analog of the classical energy, (3) discuss the evolution equation and boundary conditions, and (4) extend the energy to account for head-to-tail symmetry.
- In Section 4, we incorporate the effects of different moduli for bend and splay.
- In Section 5, we examine the structure of disclinations, and the role of bend and splay in the stability of integer vs. half-integer disclinations.
- In Section 6, we examine the coalescence of a $+\frac{1}{2}$ disclination and $-\frac{1}{2}$ disclination coming together.

1.2 Notation, Definitions and Values of Model Parameters

Boldface denotes vectors and tensors. We have used Einstein convention, i.e. repeated indices imply summation over those indices, except when noted.

Hats appended to functions refer to their value at $\hat{\boldsymbol{x}}, \hat{\hat{\boldsymbol{x}}}, \ldots$, i.e. for a field $f(\boldsymbol{x})$, we write $\hat{f} \equiv f(\hat{\boldsymbol{x}}), \hat{\hat{f}} \equiv f(\hat{\hat{\boldsymbol{x}}}), \ldots$.

$\gamma_1 \equiv \alpha_3 - \alpha_2 \geq 0$ is the rotational or twist viscosity of the director. It sets the relaxation time of the director field. We set $\gamma_1 = 1$ in our model system. α_3 and α_2 are the Leslie viscosities [Ste04].

δ is a characteristic defect lengthscale, that we set to 5. Numerical calculations use a grid spacing of at least 1.

$C_\delta(|\boldsymbol{x} - \hat{\boldsymbol{x}}|)$ is the nonlocal weight function; we assume the form

$$C_\delta(|\boldsymbol{x} - \hat{\boldsymbol{x}}|) = \begin{cases} \frac{1}{\delta^2} & \text{if } |\boldsymbol{x} - \hat{\boldsymbol{x}}| < \delta \\ 0 & \text{if } |\boldsymbol{x} - \hat{\boldsymbol{x}}| \geq \delta \end{cases} \tag{1.1}$$

The normalization is appropriate for 2D.

2 Classical Model of Nematic Liquid Crystals

We briefly summarize the key features of classical nematic director dynamics to enable us to point out the key differences and similarities with our proposed nonlocal model. The classical model of nematic liquid crystals was formulated by Frank, and Ericksen and Leslie, and is very well described in [Ste04]. For simplicity, we neglect in this paper the effect of flow, i.e., we assume that the only dynamics is due to director reorientation. In addition, we use the standard assumption that the inertia associated with director reorientation is negligible.

The Frank free energy density w is in general a function of the local values of $\boldsymbol{n}$ and $\nabla \boldsymbol{n}$. The energy of the body Ω is $E[\boldsymbol{n}] = \int_\Omega w(\boldsymbol{n}, \nabla \boldsymbol{n})\, d\Omega$. We fix $\boldsymbol{n}$ or set $\epsilon_{ikl} n_{i,j} n_l \hat{\nu}_j = 0$ on the boundary $\partial\Omega$, and $|\boldsymbol{n}| = 1$.

In the simplified 1-constant approximation, $w = \frac{K}{2} |\nabla \boldsymbol{n}|^2$.

The classical approach relies on angular momentum balance [Ste04] to derive the evolution equation for $\boldsymbol{n}$. Equivalently, we can derive this using a gradient descent approach. We prefer the latter method here because it is easier to adapt to the nonlocal energy because we do not have to first identify a nonlocal torque, but can instead do so from the final form of the equation.

The gradient dynamics has the form $\gamma_1 \langle \dot{\boldsymbol{n}}, \delta \boldsymbol{n} \rangle = -\frac{d}{d\varepsilon} E[\boldsymbol{n} + \varepsilon \delta \boldsymbol{n}] \Big|_{\varepsilon=0}$. To preserve $|\boldsymbol{n}| = 1$, the variations in $\boldsymbol{n}$ must have the form $\delta n_i = \epsilon_{ijk} n_j p_k$, where p_k is arbitrary. The dynamical equation is then:

$$\gamma_1 \dot{\boldsymbol{n}} \times \boldsymbol{n} = -\left(\frac{\partial w}{\partial \boldsymbol{n}} - \operatorname{div} \frac{\partial w}{\partial \nabla \boldsymbol{n}} \right) \times \boldsymbol{n} \Rightarrow \gamma_1 \dot{\boldsymbol{n}} = -\left(\frac{\partial w}{\partial \boldsymbol{n}} - \operatorname{div} \frac{\partial w}{\partial \nabla \boldsymbol{n}} \right) + \lambda \boldsymbol{n} \tag{2.1}$$

where λ is the Lagrange multiplier conjugate to the constraint $|\boldsymbol{n}| = 1$. Enforcing $\boldsymbol{n} \cdot \boldsymbol{n} = 1 \Rightarrow \dot{\boldsymbol{n}} \cdot \boldsymbol{n} = 0$ to eliminate λ gives the dynamical equation:

$$\gamma_1 \dot{\boldsymbol{n}} = -\left(\frac{\partial w}{\partial \boldsymbol{n}} - \operatorname{div} \frac{\partial w}{\partial \nabla \boldsymbol{n}} \right) + \left(\boldsymbol{n} \cdot \frac{\partial w}{\partial \boldsymbol{n}} - \boldsymbol{n} \cdot \operatorname{div} \frac{\partial w}{\partial \nabla \boldsymbol{n}} \right) \boldsymbol{n} \tag{2.2}$$

The dissipation associated with this dynamics is:

$$\begin{aligned} -\frac{dE}{dt} &= -\int_{\boldsymbol{x}\in\Omega} \left(\frac{\partial w}{\partial \boldsymbol{n}} - \operatorname{div}\frac{\partial w}{\partial \nabla \boldsymbol{n}}\right)\cdot \dot{\boldsymbol{n}}\, d\Omega \\ &= \frac{1}{\gamma_1}\int_{\boldsymbol{x}\in\Omega} \left|\left(\frac{\partial w}{\partial \boldsymbol{n}} - \operatorname{div}\frac{\partial w}{\partial \nabla \boldsymbol{n}}\right)\right|^2 - \left(\boldsymbol{n}\cdot\frac{\partial w}{\partial \boldsymbol{n}} - \boldsymbol{n}\cdot\operatorname{div}\frac{\partial w}{\partial \nabla \boldsymbol{n}}\right)^2 \, d\Omega \geq 0 \end{aligned} \tag{2.3}$$

The dissipation is strictly non-negative[2].

Equilibrium configurations are obtained by setting $\dot{\boldsymbol{n}} = 0$. In the 1-constant energy, this gives $\epsilon_{ikl} n_{i,jj} n_l = 0$.

Alternatively, we can parametrize $\boldsymbol{n} = (\sin\theta(\boldsymbol{x}), \cos\theta(\boldsymbol{x}))$ which automatically satisfies the unit vector constraint[3]. Then, $n_{1,i} = \cos(\theta)\theta_{,i}$ and $n_{2,i} = -\sin(\theta)\theta_{,i}$, giving for 1-constant energy:

$$E[\theta] = \frac{K}{2}\int_\Omega \theta_{,i}\theta_{,i}\, d\Omega \tag{2.4}$$

The equilibrium configuration is described by $\theta_{,ii} = 0$ in Ω, with boundary conditions $\theta = \theta_0$ or $\theta_{,i}\nu_i = 0$ at each point on the boundary $\partial\Omega$. The description in terms of θ has the advantage that the unit vector constraint is exactly satisfied at all times for numerical solutions that discretize in time and use finite time steps. The description in terms of $\boldsymbol{n}$ will require a careful projection scheme at each time step to bring the director back to the unit sphere. Our approach for the nonlocal energy will be to formulate in terms of a unit vector field $\boldsymbol{n}$, but use θ for the numerical solution.

The head-tail symmetry is important to describe half-integer disclinations: even away from the core, there is a line (in 2D) across which the sense changes by π. Using either θ or a vector field for $\boldsymbol{n}$ does not allow us to do this easily with the classical energy, but will be possible with the proposed nonlocal regularization.

3 Nonlocal Regularized Free Energy Without Gradients

Our nonlocal regularized energy is motivated by the peridynamic model for fracture [Sil00, SL10] with some key differences. Peridynamics has provided an important model for fracture calculations because of the key feature that spatial derivatives are not required in the theory, hence allowing for discontinuous displacement fields.

3.1 A Motivating One-Dimensional Example

Consider the operator $\tilde{D}$ that acts on a function f as defined:

$$\tilde{D}f(x) = \frac{3}{2\delta^3}\int_{x-\delta}^{x+\delta} \left(f(x) - f(\hat{x})\right)(x-\hat{x})\; d\hat{x} \tag{3.1}$$

[2] Gradient dynamics with a unit vector constraint is not necessarily dissipative. The Landau-Lifshitz-Gilbert (LLG) dynamics in micromagnetism (e.g., [AKST14]) is given by $\langle \dot{\boldsymbol{n}}, \boldsymbol{p}\rangle = -\left.\frac{d}{d\varepsilon} E\left[\boldsymbol{n} + \varepsilon\delta\boldsymbol{n}\right]\right|_{\varepsilon=0}$ with $\delta n_i = \epsilon_{ijk} n_j p_k$, where p_k is arbitrary, in the undamped case. The inner product above is not the same as the Ericksen-Leslie dynamics, and it can be shown that the energy in the undamped LLG dynamics is conserved.

[3] This is in 2D, but the extension to 3D is straightforward.

When $f(x) = Ax + B$, we evaluate $\tilde{D}f(x) = A$. For linear functions, $\tilde{D}f$ matches the derivative. Consider the Taylor expansion $f(x) - f(\hat{x}) = (x - \hat{x})f'(x) + \frac{1}{2}(x - \hat{x})^2 f''(x) + \ldots$. Then, $\tilde{D}f(x) = f'(x) + C_3\delta^2 f'''(x) + \ldots$, where the even derivatives vanish by symmetry. Therefore, the operator $\tilde{D}$ provides an approximation to the derivative when δ and the higher derivatives are sufficiently small. However, when f is not smooth such as at a discontinuity or other singularity where the derivatives are not well-defined, the original integral expression continues to be well-defined.

Physically, the operator can be understood as averaging the slope of f over a neighborhood of x of size δ, i.e., averaging $\dfrac{f(x) - f(\hat{x})}{x - \hat{x}}$. However, to avoid singularities from the denominator, we use the weight $(x - \hat{x})^2$ in the process of averaging. When the slope is constant, i.e. a linear function, we recover exactly the derivative; when the function is slowly varying, we get higher-order regularizing terms; and when the function does not have well-defined derivatives, we obtain a finite value that is physically related to the average slope in the neighborhood.

While $\tilde{D}f$ provides an attractive alternative to the derivative df/dx, there is one key drawback. The derivative $df/dx = 0$ only when $f = \text{const.}$ and not otherwise. However, while $\tilde{D}f = 0$ when $f = \text{const.}$, it can also be 0 for other functions; in fact, any non-constant function that is antisymmetric about x will have the slopes exactly cancel out to give an average value of 0. Therefore, one can have spurious soft modes with zero energy that have no physical basis.

To get around this, we first observe that the free energy density consists of terms that are all components of the gradient raised to the second power [Ste04]. In the specific case of the 1-constant energy, the energy density is simply the gradient squared. In one dimension, this would require us to approximate $\left(\dfrac{df}{dx}\right)^2$. Motivated by the discussion immediately above, the operator

$$\tilde{D}_2 f(x) \sim \int_{x-\delta}^{x+\delta} \left(\frac{f(x) - f(\hat{x})}{x - \hat{x}}\right)^2 d\hat{x} \tag{3.2}$$

would provide a nonlocal regularized approximation up to normalization. The integrand is always non-negative, thereby not allowing any cancellations. For $\tilde{D}_2 f(x)$ to evaluate to 0, the integrand must be 0 everywhere, ensuring that $f = \text{const.}$ is the only possibility.

3.2 Nonlocal Regularization in Three Dimensions

Following ideas from peridynamics [Sil00], we write the nonlocal analog to the Frank energy as:

$$E[\boldsymbol{n}] = \frac{K}{2} \int_{\boldsymbol{x}\in\Omega} \int_{\hat{\boldsymbol{x}}\in\Omega} \frac{1}{2} C_\delta(\boldsymbol{x}, \hat{\boldsymbol{x}}) \, (\hat{n}_i - n_i) \, \frac{\hat{x}_j - x_j}{|\hat{\boldsymbol{x}} - \boldsymbol{x}|} \, (\hat{n}_i - n_i) \, \frac{\hat{x}_j - x_j}{|\hat{\boldsymbol{x}} - \boldsymbol{x}|} \, dV_{\hat{\boldsymbol{x}}} \, dV_{\boldsymbol{x}} \tag{3.3}$$

where C_δ is a function that is symmetric in the arguments.

What motivates this expression? The classical gradient is the vector pointing in the direction in which the increase of η is maximum. Our expression examines the change in $\boldsymbol{n}$ between $\boldsymbol{x}$ and every point $\hat{\boldsymbol{x}}$ in Ω, and weights the direction $\hat{\boldsymbol{x}} - \boldsymbol{x}$ by the change in that direction; the larger the increase, the greater the weight for that direction. So the direction of largest increase features most prominently in the average.

It is natural for points $\hat{\boldsymbol{x}}$ that are closer to $\boldsymbol{x}$ to play a larger role in the averaging, and this weighting is introduced by the function $C_\delta(\boldsymbol{x}, \hat{\boldsymbol{x}})$. This introduces a lengthscale, denoted δ, into our model that is not

present in the classical Frank free energy. In this paper, we will restrict ourselves to isotropic and spatially homogeneous systems, and hence we will write $C_\delta(|\boldsymbol{x}-\hat{\boldsymbol{x}}|)$. Further, we use C_δ to introduce a cut-off distance, i.e. $C_\delta(|\boldsymbol{x}-\hat{\boldsymbol{x}}|)=0$ when $|\boldsymbol{x}-\hat{\boldsymbol{x}}|>\delta$. Finally, for conciseness, we absorb $\frac{\hat{x}_j-x_j}{|\hat{\boldsymbol{x}}-\boldsymbol{x}|}\cdot\frac{\hat{x}_j-x_j}{|\hat{\boldsymbol{x}}-\boldsymbol{x}|}$ in (3.3) within C_δ by redefining it appropriately, but retaining the same symbol for convenience. Putting this together, we can write:

$$E[\boldsymbol{n}]=\frac{K}{2}\int_{\boldsymbol{x}\in\Omega}\int_{\hat{\boldsymbol{x}}\in\Omega}\frac{1}{2}C_\delta(|\boldsymbol{x}-\hat{\boldsymbol{x}}|)\cdot(\hat{\boldsymbol{n}}-\boldsymbol{n})^2\;dV_{\hat{\boldsymbol{x}}}\;dV_{\boldsymbol{x}} \tag{3.4}$$

We now consider a physical interpretation of (3.4). From a physical perspective, the classical Frank model states that there is an energetic cost to molecules not being aligned with each other. Loosely, it penalizes changes in the molecular orientations at "adjacent" material points, and in the limit this becomes the gradient. Our model compares the molecular orientation at a point $\boldsymbol{x}$ with the molecular orientation at every point $\hat{\boldsymbol{x}}$ contained in Ω. To leading order, the energy contained in the interaction between molecules at these points is $\frac{1}{2}C_\delta(|\boldsymbol{x}-\hat{\boldsymbol{x}}|)\left(\boldsymbol{n}(\boldsymbol{x})-\boldsymbol{n}(\hat{\boldsymbol{x}})\right)^2$, where $C_\delta(\boldsymbol{x},\hat{\boldsymbol{x}})$ is analogous to a spring constant and depends on the distance between the points. The total free energy simply sums over all pairs of molecules in Ω, with an additional factor of $\frac{1}{2}$ to correct for double-counting of bonds. While molecular interactions are typically very local, in homogeneous non-defect regions we can think of the molecular interactions as being renormalized.

From the perspective of the classical model of nematic liquid crystals, our model introduces a new lengthscale δ. This sets a material lengthscale, and corresponds to the scaling of the core radius of a disclination defect. There is a close analogy to the relation between classical elasticity – which has no lengthscale – and gradient or peridynamics models of elasticity which introduce lengthscales [SL10]; in the latter class of models, defects such as interfaces and dislocations then can inherit this lengthscale as a "core radius". In a calculation with application to a real material, the lengthscale introduced could be taken to scale with the defect size. An appropriate choice could be the lengthscale parameter that appears in the Q-tensor models.

3.3 Accounting for Head-Tail Symmetry

Typical nematic liquid crystal molecules are non-polar and have head-tail symmetry. That is, changing $\boldsymbol{n}\leftrightarrow-\boldsymbol{n}$ should not change any physical quantities. This is particularly important in half-integer disclinations, e.g. Fig. 1, where there is a plane – or line in 2D – across which the sense of the director changes. If represented by a unit vector field, the vector flips head-to-tail; if represented by θ in 2D, there is discontinuity of π. These discontinuities should not contribute to the energy or equilibrium equation. However, the energy in (3.4) is sensitive to such a transformation. We now discuss how to modify the energy to reflect the physics.

Consider two directors that are within δ. The minimum energy configuration is $\boldsymbol{n}_1\cdot\boldsymbol{n}_2=1$ (they are parallel). The highest energy configuration is $\boldsymbol{n}_1\cdot\boldsymbol{n}_2=0$ (they are normal). We further want that the configuration $\boldsymbol{n}_1\cdot\boldsymbol{n}_2=-1$ (they are anti-parallel) is a minimum energy state, with the same energy as the parallel state. Some choices of energy that satisfies this are $-|\boldsymbol{n}_1\cdot\boldsymbol{n}_2|\equiv-|\cos(\theta_1-\theta_2)|$, $-(\boldsymbol{n}_1\cdot\boldsymbol{n}_2)^2\equiv-\cos^2(\theta_1-\theta_2)$, etc.

Consider now the integrand from (3.4). We can write $(\boldsymbol{n}-\hat{\boldsymbol{n}})^2=2-2\boldsymbol{n}\cdot\hat{\boldsymbol{n}}=2-2\cos(\theta-\hat{\theta})$. Since it is

an energy, we can ignore constants and write the energy as $-2\boldsymbol{n}\cdot\hat{\boldsymbol{n}} = -2\cos(\theta-\hat{\theta})$. From the discussion in the previous paragraph, it is clear that this does not behave well when $\boldsymbol{n}$ and $\hat{\boldsymbol{n}}$ are anti-parallel, and shows the problem with (3.4).

Based on these physical considerations, we replace the integrand in nonlocal energy density by $-\left|2-(\boldsymbol{n}-\hat{\boldsymbol{n}})^2\right| = -2\left|\boldsymbol{n}\cdot\hat{\boldsymbol{n}}\right|$. That is, we propose the following nonlocal regularized free energy:

$$E[\boldsymbol{n}] = \frac{K}{2}\int_{\boldsymbol{x}\in\Omega} \underbrace{\int_{\hat{\boldsymbol{x}}\in\Omega} \frac{1}{2}C_\delta(|\boldsymbol{x}-\hat{\boldsymbol{x}}|)\cdot -\left|2-(\boldsymbol{n}-\hat{\boldsymbol{n}})^2\right| \, dV_{\hat{\boldsymbol{x}}}}_{\text{free energy density at } \boldsymbol{x}} \, dV_{\boldsymbol{x}} \tag{3.5}$$

This recovers the classical model when the anti-parallel nature is not an issue because it is quadratic in $\boldsymbol{n}-\hat{\boldsymbol{n}}$. It is obvious that our proposed expression does not impose any continuity requirements on $\boldsymbol{n}$. The energy density – and therefore the total energy – is bounded and well-defined even if $\boldsymbol{n}$ has all kinds of discontinuities, as long as $\boldsymbol{n}$ itself remains bounded; this is automatic due to the unit vector constraint. It is also obvious that the energy density is non-zero except for constant fields if we restrict $C_\delta(|\boldsymbol{x}-\hat{\boldsymbol{x}}|) \geq 0$ because the integrand is non-negative.

We begin with an energy that is quadratic in the nonlocal gradient operator. However, this does not respect head-tail symmetry when we use a vector field $\boldsymbol{n}$. To get around this, we modify the nonlocal gradient operator directly following ideas from Maier-Saupe theory and related models such as the Gay-Berne and Lebwohl-Lasher models, e.g. [HDCK12], Chapter 4 in [PB94], [LL72], [PP01], [A$^+$93], from a vast body of work. This closely follows more sophisticated approaches proposed by [BB15] and [ZZA$^+$] who use non-convexity in the gradient of the director to achieve similar ends.

We could, in principle, use many other expressions that resolve the head-tail issue, e.g. $-2(\boldsymbol{n}\cdot\hat{\boldsymbol{n}})^2$ for the free energy density. But these would not recover the classical model in the limit.

3.4 Equilibrium and Evolution Equations

The equilibrium equation is obtained from setting the functional derivative of the energy from (3.5) to 0. That is, $\dfrac{d}{d\varepsilon}E\left[\boldsymbol{n}+\varepsilon\delta\boldsymbol{n}\right]\Big|_{\varepsilon=0} = 0$. To satisfy the unit vector constraint on $\boldsymbol{n}$, we use the variation $\delta n_i = \epsilon_{ijk}n_j p_k$ where $\boldsymbol{p}$ is an arbitrary vector field. This gives:

$$\begin{aligned}
0 &= \frac{K}{2}\int_{\boldsymbol{x}\in\Omega}\int_{\hat{\boldsymbol{x}}\in\Omega} C_\delta(|\boldsymbol{x}-\hat{\boldsymbol{x}}|)\cdot\operatorname{sign}(2-(\boldsymbol{n}-\hat{\boldsymbol{n}})^2)\cdot\epsilon_{ijk}\left(n_i-\hat{n}_i\right)\left(n_j p_k-\hat{n}_j\hat{p}_k\right)\, dV_{\hat{\boldsymbol{x}}}\, dV_{\boldsymbol{x}} \\
&= \frac{K}{2}\int_{\boldsymbol{x}\in\Omega}\int_{\hat{\boldsymbol{x}}\in\Omega} C_\delta(|\boldsymbol{x}-\hat{\boldsymbol{x}}|)\cdot\operatorname{sign}(2-(\boldsymbol{n}-\hat{\boldsymbol{n}})^2)\cdot\epsilon_{ijk}\left(n_i-\hat{n}_i\right)n_j p_k\, dV_{\hat{\boldsymbol{x}}}\, dV_{\boldsymbol{x}} \\
&\quad - \frac{K}{2}\int_{\boldsymbol{x}\in\Omega}\int_{\hat{\boldsymbol{x}}\in\Omega} C_\delta(|\boldsymbol{x}-\hat{\boldsymbol{x}}|)\cdot\operatorname{sign}(2-(\boldsymbol{n}-\hat{\boldsymbol{n}})^2)\cdot\epsilon_{ijk}\left(n_i-\hat{n}_i\right)\hat{n}_j\hat{p}_k\, dV_{\hat{\boldsymbol{x}}}\, dV_{\boldsymbol{x}} \\
&= K\int_{\boldsymbol{x}\in\Omega} p_k\int_{\hat{\boldsymbol{x}}\in\Omega} C_\delta(|\boldsymbol{x}-\hat{\boldsymbol{x}}|)\cdot\operatorname{sign}(2-(\boldsymbol{n}-\hat{\boldsymbol{n}})^2)\cdot\epsilon_{ijk}\left(n_i-\hat{n}_i\right)n_j\, dV_{\hat{\boldsymbol{x}}}\, dV_{\boldsymbol{x}}
\end{aligned} \tag{3.6}$$

where we have relabeled $\boldsymbol{x}\leftrightarrow\hat{\boldsymbol{x}}$ to combine integrals in the second line.

Using that p_k is an arbitrary field, we eliminate the integration over $\boldsymbol{x}$:

$$\epsilon_{ijk}n_j\int_{\hat{\boldsymbol{x}}\in\Omega} C_\delta(|\boldsymbol{x}-\hat{\boldsymbol{x}}|)\cdot\operatorname{sign}(2-(\boldsymbol{n}-\hat{\boldsymbol{n}})^2)\cdot\left(n_k-\hat{n}_k\right)\, dV_{\hat{\boldsymbol{x}}} = 0 \tag{3.7}$$

We compare this with the statement of equilibrium in the classical 1-constant model: $\epsilon_{ijk} n_j n_{k,ll} = 0$.

In 2D, an orientational description $\boldsymbol{n} = (\sin\theta(\boldsymbol{x}), \cos\theta(\boldsymbol{x}))$ gives:

$$E[\theta] = \frac{K}{2} \int_{\boldsymbol{x}\in\Omega} \int_{\hat{\boldsymbol{x}}\in\Omega} \frac{1}{2} C_\delta(|\boldsymbol{x}-\hat{\boldsymbol{x}}|) \left(1 - |\cos(\hat{\theta}-\theta)|\right) \, dV_{\hat{\boldsymbol{x}}} \, dV_{\boldsymbol{x}} \tag{3.8}$$

for the energy, and equilibrium configurations are described by:

$$K \int_{\hat{\boldsymbol{x}}\in\Omega} C_\delta(|\boldsymbol{x}-\hat{\boldsymbol{x}}|) \operatorname{sign}\left[\cos(\theta-\hat{\theta})\right] \, \sin(\hat{\theta}-\theta) \, dV_{\hat{\boldsymbol{x}}} = 0 \tag{3.9}$$

As in the classical case, we deduce the evolution equation using $\gamma_1 \langle \dot{\boldsymbol{n}}, \delta\boldsymbol{n}\rangle = -\frac{d}{d\varepsilon} E\left[\boldsymbol{n} + \varepsilon\delta\boldsymbol{n}\right]\Big|_{\varepsilon=0}$ using the variation $\delta n_i = \epsilon_{ijk} n_j p_k$, where $\boldsymbol{p}$ is arbitrary. This gives us:

$$\begin{aligned} \gamma_1 \dot{\boldsymbol{n}} \times \boldsymbol{n} &= \left(K \int_{\hat{\boldsymbol{x}}\in\Omega} C_\delta(|\boldsymbol{x}-\hat{\boldsymbol{x}}|) \cdot \operatorname{sign}(2-(\boldsymbol{n}-\hat{\boldsymbol{n}})^2) \cdot (\boldsymbol{n}-\hat{\boldsymbol{n}}) \, dV_{\hat{\boldsymbol{x}}} \, dV_{\boldsymbol{x}} \right) \times \boldsymbol{n} \\ \Rightarrow \gamma_1 \dot{\boldsymbol{n}} &= K \int_{\hat{\boldsymbol{x}}\in\Omega} C_\delta(|\boldsymbol{x}-\hat{\boldsymbol{x}}|) \cdot \operatorname{sign}(2-(\boldsymbol{n}-\hat{\boldsymbol{n}})^2) \cdot (\boldsymbol{n}-\hat{\boldsymbol{n}}) \, dV_{\hat{\boldsymbol{x}}} \, dV_{\boldsymbol{x}} + \lambda \boldsymbol{n} \end{aligned} \tag{3.10}$$

Enforcing $\boldsymbol{n}\cdot\boldsymbol{n} = 1 \Rightarrow \dot{\boldsymbol{n}}\cdot\boldsymbol{n} = 0$ to eliminate λ gives:

$$\gamma_1 \dot{\boldsymbol{n}} = (\boldsymbol{I} - \boldsymbol{n}\otimes\boldsymbol{n}) \cdot K \int_{\hat{\boldsymbol{x}}\in\Omega} C_\delta(|\boldsymbol{x}-\hat{\boldsymbol{x}}|) \cdot \operatorname{sign}(2-(\boldsymbol{n}-\hat{\boldsymbol{n}})^2) \cdot (\boldsymbol{n}-\hat{\boldsymbol{n}}) \, dV_{\hat{\boldsymbol{x}}} \, dV_{\boldsymbol{x}} \tag{3.11}$$

The corresponding 2D orientational description is:

$$-K \int_{\hat{\boldsymbol{x}}\in\Omega} C_\delta(|\boldsymbol{x}-\hat{\boldsymbol{x}}|) \operatorname{sign}\left[\cos(\theta-\hat{\theta})\right] \, \sin(\hat{\theta}-\theta) \, dV_{\hat{\boldsymbol{x}}} = \dot{\theta} \tag{3.12}$$

The dissipation associated with the nonlocal model can be computed:

$$\begin{aligned} -\frac{dE}{dt} &= \frac{K}{2} \int_{\boldsymbol{x}\in\Omega} \int_{\hat{\boldsymbol{x}}\in\Omega} C_\delta(|\boldsymbol{x}-\hat{\boldsymbol{x}}|) \cdot \operatorname{sign}\left(2-(\boldsymbol{n}-\hat{\boldsymbol{n}})^2\right) \cdot (\boldsymbol{n}-\hat{\boldsymbol{n}}) \cdot \left(\dot{\boldsymbol{n}} - \dot{\hat{\boldsymbol{n}}}\right) \, dV_{\hat{\boldsymbol{x}}} \, dV_{\boldsymbol{x}} \\ &= K \int_{\boldsymbol{x}\in\Omega} \dot{\boldsymbol{n}} \cdot \int_{\hat{\boldsymbol{x}}\in\Omega} C_\delta(|\boldsymbol{x}-\hat{\boldsymbol{x}}|) \cdot \operatorname{sign}\left(2-(\boldsymbol{n}-\hat{\boldsymbol{n}})^2\right) \cdot (\boldsymbol{n}-\hat{\boldsymbol{n}}) \, dV_{\hat{\boldsymbol{x}}} \, dV_{\boldsymbol{x}} \\ &= \frac{1}{\gamma_1} \int_{\boldsymbol{x}\in\Omega} \boldsymbol{A} \cdot (\boldsymbol{I} - \boldsymbol{n}\otimes\boldsymbol{n}) \cdot \boldsymbol{A} \, dV_{\boldsymbol{x}} \end{aligned} \tag{3.13}$$

where $\boldsymbol{A} := K \int_{\hat{\boldsymbol{x}}\in\Omega} C_\delta(|\boldsymbol{x}-\hat{\boldsymbol{x}}|) \cdot \operatorname{sign}\left(2-(\boldsymbol{n}-\hat{\boldsymbol{n}})^2\right) \cdot (\boldsymbol{n}-\hat{\boldsymbol{n}}) \, dV_{\hat{\boldsymbol{x}}}$. Since $\boldsymbol{I} - \boldsymbol{n}\otimes\boldsymbol{n}$ is positive semi-definite, it follows that the dissipation is always non-negative.

3.5 Boundary Conditions

As in the peridynamic model of elasticity, boundary conditions cannot be applied in the classical sense. Roughly, imposing conditions on the boundary – a set of measure 0 in the integral – provides an infinitesimal contribution to the integral. However, a physically-natural solution to this issue is to instead

impose conditions over a layer of finite thickness – with thickness of order δ – on the boundary. Given that in our model molecules interact over a finite range, it is natural to provide boundary conditions with more structure than holding them fixed on a low-dimensional set (the boundary). For instance, to impose that the nematic molecules have a specific orientation on the boundary, we hold the orientation fixed for all molecules within the boundary layer region. That is, $\theta(\boldsymbol{x}) = \theta_0 \ \forall \boldsymbol{x} \in \Omega_{bl}$ where Ω_{bl} is a portion of the Ω with finite volume. In this paper, this is the only type of boundary condition that we use, but other boundary conditions can be similarly smeared-out following the techniques used in peridynamics [Sil00, SL10, DB06].

4 Bend and Splay: Extension Beyond the 1-Constant Energy

In the classical 1-constant model, a single modulus K defines the energy in the bend, splay, and twist modes. The more general Frank free energy has different moduli for each of these modes. We examine the same issue in the nonlocal regularized energy. We restrict ourselves to 2D and therefore only distinguish between bend and splay, but an extension to 3D that also incorporates twist is conceptually analogous. Appendix A discusses briefly an alternative strategy.

The physical basis for 3 different moduli is seen from Fig. 2. We can differentiate between these modes as follows. Splay can be differentiated from both bend and twist by noticing that the quantity $(\boldsymbol{n}-\hat{\boldsymbol{n}})\cdot(\boldsymbol{x}-\hat{\boldsymbol{x}})$ is 0 for both bend and twist, but is nonzero – and can be normalized to 1 – for splay. Similarly, bend can be differentiated from both splay and twist by using the quantity $\boldsymbol{n}\cdot(\boldsymbol{x}-\hat{\boldsymbol{x}})$, which is 0 for both splay and twist but is nonzero and normalizable to 1 for bend.

Since we are currently only working in 2D and considering only bend and splay modes, we need only differentiate these 2 modes here. We write for the modulus $K = K_s\left(1-\left|\boldsymbol{n}\cdot\hat{\delta\boldsymbol{x}}\right|\right) + K_b\left|\boldsymbol{n}\cdot\hat{\delta\boldsymbol{x}}\right|$, where $\hat{\delta\boldsymbol{x}} \equiv \dfrac{\hat{\boldsymbol{x}}-\boldsymbol{x}}{|\hat{\boldsymbol{x}}-\boldsymbol{x}|}$. Then, K_s is the coefficient for splay and K_b is the coefficient for bending. When $\boldsymbol{n}\cdot\hat{\delta\boldsymbol{x}} = 0$, then we have splay, and when $\boldsymbol{n}\cdot\hat{\delta\boldsymbol{x}} = 1$ we have bending.

Using the orientational description for compactness, the energy can now be written:

$$E[\theta] = \int_{\boldsymbol{x}\in\Omega}\int_{\hat{\boldsymbol{x}}\in\Omega} \frac{K(\theta,\boldsymbol{x},\hat{\boldsymbol{x}})}{2}\cdot\frac{1}{2}C_\delta(|\boldsymbol{x}-\hat{\boldsymbol{x}}|)\left(1-|\cos(\hat{\theta}-\theta)|\right)\,dV_{\hat{\boldsymbol{x}}}\,dV_{\boldsymbol{x}} \tag{4.1}$$

We can also identify the bending and splay contributions individually:

$$\begin{aligned} E[\theta] = &\underbrace{\frac{1}{2}K_b\int_{\boldsymbol{x}\in\Omega}\int_{\hat{\boldsymbol{x}}\in\Omega}\frac{1}{2}C_\delta(|\boldsymbol{x}-\hat{\boldsymbol{x}}|)\left|\boldsymbol{n}\cdot\hat{\delta\boldsymbol{x}}\right|\left(1-|\cos(\hat{\theta}-\theta)|\right)\,dV_{\hat{\boldsymbol{x}}}\,dV_{\boldsymbol{x}}}_{\text{bend}} \\ &+\underbrace{\frac{1}{2}K_s\int_{\boldsymbol{x}\in\Omega}\int_{\hat{\boldsymbol{x}}\in\Omega}\frac{1}{2}C_\delta(|\boldsymbol{x}-\hat{\boldsymbol{x}}|)\left(1-\left|\boldsymbol{n}\cdot\hat{\delta\boldsymbol{x}}\right|\right)\left(1-|\cos(\hat{\theta}-\theta)|\right)\,dV_{\hat{\boldsymbol{x}}}\,dV_{\boldsymbol{x}}}_{\text{splay}} \end{aligned} \tag{4.2}$$

The evolution equation is obtained from a gradient descent based on θ without any constraints:

$$-\int_{\hat{\boldsymbol{x}}\in\Omega} C_\delta(|\boldsymbol{x}-\hat{\boldsymbol{x}}|)\left(\frac{dK}{d\theta}\cdot\left(1-|\cos(\hat{\theta}-\theta)|\right)+K(\theta)\cdot\operatorname{sign}\left[\cos(\theta-\hat{\theta})\right]\,\sin(\hat{\theta}-\theta)\right)\,dV_{\hat{\boldsymbol{x}}} = \dot{\theta} \tag{4.3}$$

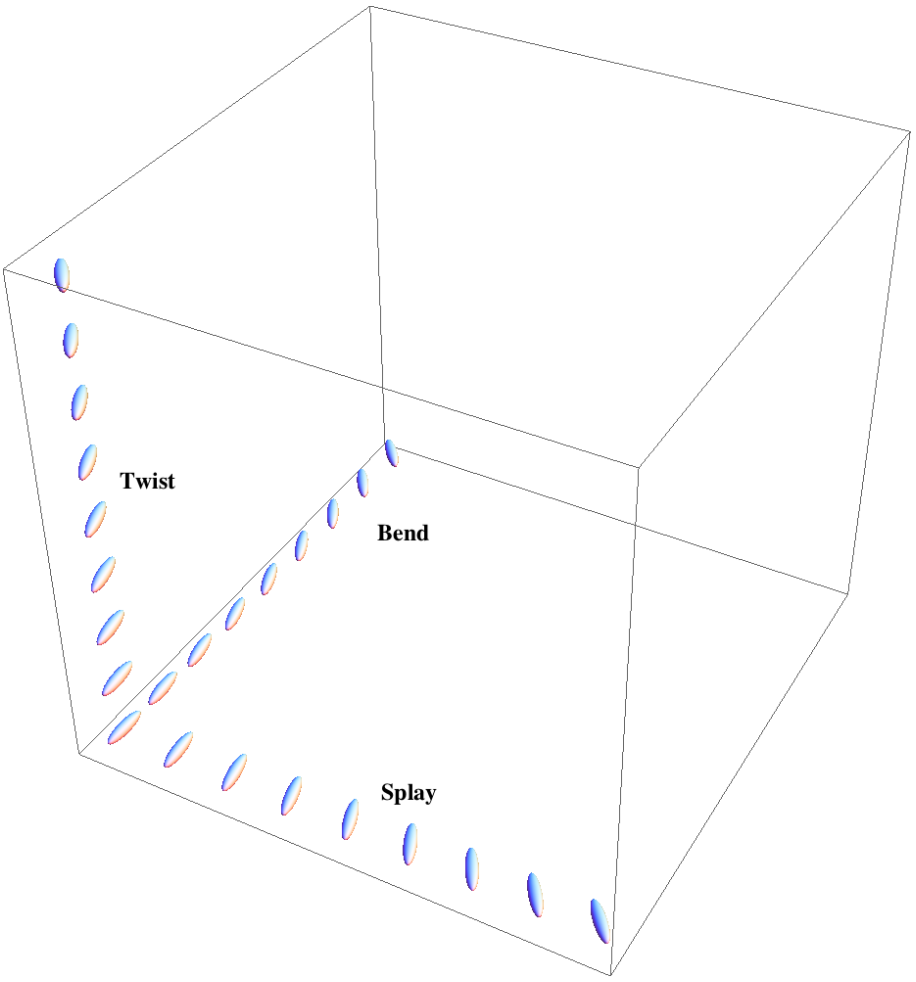

Figure 2: Bend, Splay and Twist modes. These modes can be differentiated in our nonlocal model by using the quantities $(\boldsymbol{n} - \hat{\boldsymbol{n}}) \cdot (\boldsymbol{x} - \hat{\boldsymbol{x}})$ and $\boldsymbol{n} \cdot (\boldsymbol{x} - \hat{\boldsymbol{x}})$. When normalized, these quantities are both 0 for twist, 0 and 1 respectively for bend, and 1 and 0 respectively for splay.

The equilibrium equation is obtained by setting the right side above to 0.

5 Structure and Stability of Individual Disclinations

We use the model to examine the stability and structure of various half-integer and integer disclinations. We examine these using the 1-constant nonlocal energy as well as the energy that differentiates between bend and splay.

5.1 The 1-Constant Nonlocal Energy

In the 1-constant nonlocal energy, we find that only $\pm\frac{1}{2}$ disclinations are stable; disclinations of higher strength always split into the appropriate number of $\pm\frac{1}{2}$ disclinations. We show some examples of this below.

In all of these calculations, we use a discretization mesh size of 1 with $\delta = 5$, except where stated otherwise. We have tested with finer discretizations going down to 0.01 to ensure that our approximation is accurate. We use a square domain with size 200×200. For the starting configuration, we use the classical formula for a disclination $\boldsymbol{n}(\boldsymbol{x}) = (\sin(k\theta_0(\boldsymbol{x}) + \alpha), \cos(k\theta_0(\boldsymbol{x}) + \alpha),$ where $\tan\theta_0 = x_2/x_1$, and then evolve using the equations presented above. The initial and final configurations are shown in Fig. 3.

This finding agrees qualitatively with calculations in [MHML05, BKŽ98] which use the Q-tensor and molecular dynamics methods respectively, in that only $\pm\frac{1}{2}$ defects are stable in the 1-constant energy. It is consistent also with the heuristic that the energy of a disclination scales with the square of the charge that it carries [dP95], as well as rigorous work [BPP12].

While the final states are largely in agreement with other aproaches, the dynamics is qualitatively different in our model compared to the Q-tensor calculations from [MHML05]. They find that a $+2$ defect first splits into two $+1$ defects, and then splits a second time into four $+\frac{1}{2}$ defects. In our calculations, all of the defects split almost instantly into $\pm\frac{1}{2}$ disclinations that are then repelled from each other and move apart. While their geometry is circular and hence different from our square domain, in both their work and ours the domain is large enough that it is unlikely that this is the reason for the difference. It is likely a consequence of the differences between the evolution equations in the Ericksen-Leslie model with our energy vs. the Q-tensor model.

We also notice that the energy (3.4) has stable ± 1 disclinations and does not form $\pm\frac{1}{2}$ disclinations. However, this occurs due to the unphysical feature that the lack of head-tail symmetry associates a very high energy to the line (in 2D) across which the director changes sense that accompanies $\pm\frac{1}{2}$ disclinations.

We then examine the detailed structure of the core for $\pm\frac{1}{2}$ defects. For these calculations, we use a much finer discretization of 0.1 with the same value of δ. In an initial set of calculations, we began with the classical solution as above, and evolved to find the relaxed configuration. The solutions in our model are extremely close to the starting classical solution, and the changes are dominated by numerical discretization errors. So we instead use as initial the classical solution everywhere outside a core region of radius 2; within this region, we set all directors to point vertically. The director field relaxes to a solution that is again very similar to the classical solution, but the disclination translates during the relaxation due to the severe perturbation that we have induced in the initial conditions. We therefore perform a best fit of the relaxed configuration against the formula for a translated disclination, treating the disclination center as the parameters to optimize over. Fig. 4 shows the change in the director angle. The difference between our solution and the classical disclination solution is confined to the core region, and even there is small.

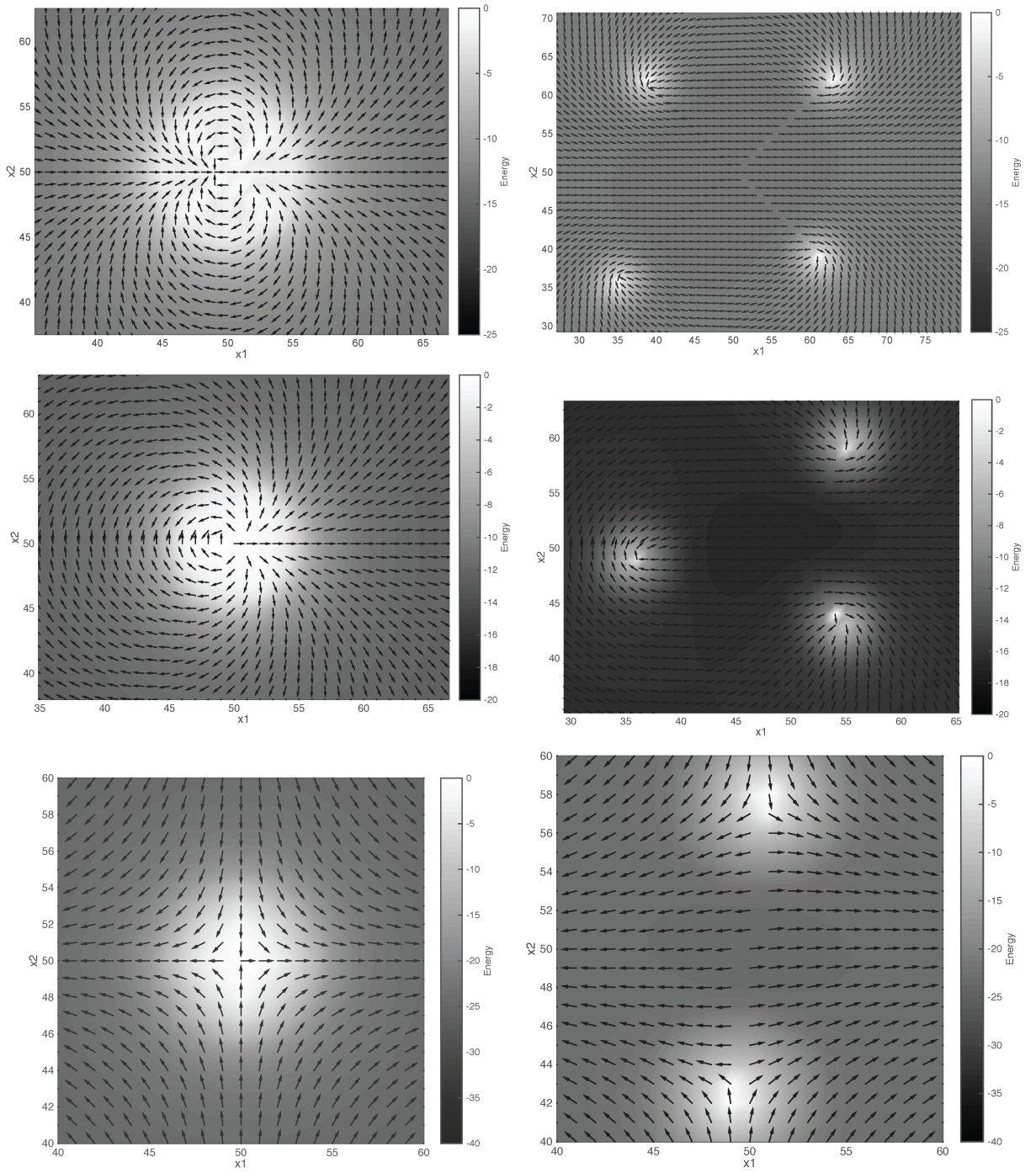

Figure 3: Top: A $+2$ disclination constructed using the classical solution (left), and the final configuration of four well-separated $+\frac{1}{2}$ disclinations (right). Middle: The similar process for a $+3/2$ disclination decomposing into three $+\frac{1}{2}$ disclinations. Bottom: A -1 disclination decomposing into two $-\frac{1}{2}$ disclinations. The vector field is overlaid on the energy density. We observe similar decompositions in $+1, -3/2$, and other disclinations stronger than $\pm\frac{1}{2}$.

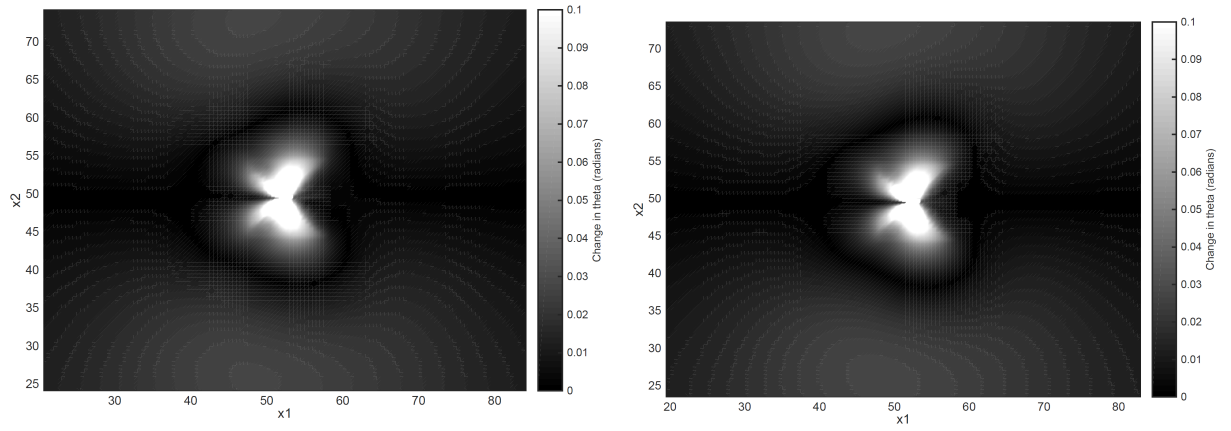

Figure 4: Angular difference between a classical disclination solution and our relaxed disclination configuration for $+\frac{1}{2}$ (left) and $-\frac{1}{2}$ (right). Outside the core, the classical solution and our relaxed solution are practically identical. Note the scale: the difference is extremely small.

5.2 Disclinations in the Bend-Splay Energy

In the previous subsection, we see that the nonlocal 1-constant energy has only $\pm\frac{1}{2}$ disclinations. In experiments, however, it has been noticed that ± 1 defects dissociate into two closely-spaced $\pm\frac{1}{2}$ cores [MPR14]. As described in [YR02], the dissociation of ± 1 disclinations is controlled by the ratio of bend to splay energies. Looking at Fig. 1, we see that the $+1$ disclination is dominated by bend, whereas the $+\frac{1}{2}$ disclination has a significant amount of both splay and bend. We notice that in our approach to differentiating between bend and splay based on $\boldsymbol{n} \cdot (\boldsymbol{x} - \hat{\boldsymbol{x}})$, there will be some level of splay character in the core region of the classical $+1$ defect.We examine the behavior of a $+1$ disclination in our model at two limits, one with $K_s = 10K_b$ and the other with $K_s = 0.1K_b$.

We first plot the partitioning of energy between bend and splay in the classical solution with $K_b = K_s$ in Fig. 5. As we expect, the bending energy is generally dominant, though the splay energy is not vanishing as explained above.

We then evolve the director field from this initial configuration. In the case when the bending modulus is large compared to the splay modulus ($K_b \gg K_s$), bending is expensive energetically and hence the system dissociated into two $+\frac{1}{2}$ disclinations in which some of the distortion can be accommodated as splay (Fig. 6, top). In the case when the bending modulus is small compared to the splay modulus ($K_b \ll K_s$), bending is not expensive and hence the system retains roughly the original disclination configuration thereby reducing the amount of splay (Fig. 6, bottom). Intermediate configurations between these two limits lead to partially dissociated disclinations that are qualitatively comparable to the observations in [MPR14] and the theoretical model in [YR02].

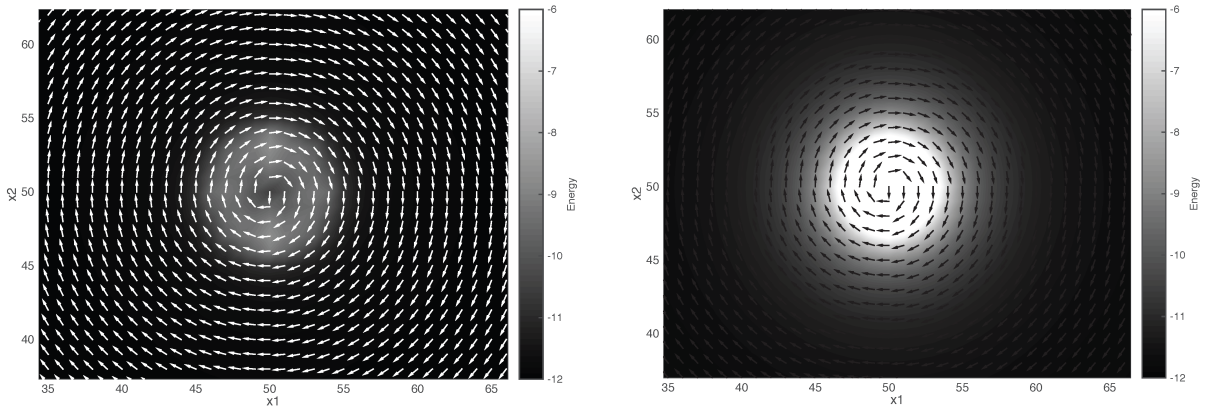

Figure 5: Partitioning of the energy into splay (left) and bend (right) energies with $K_b = K_s$. The bending distortion has significantly higher energy. Both are localized around the disclination core.

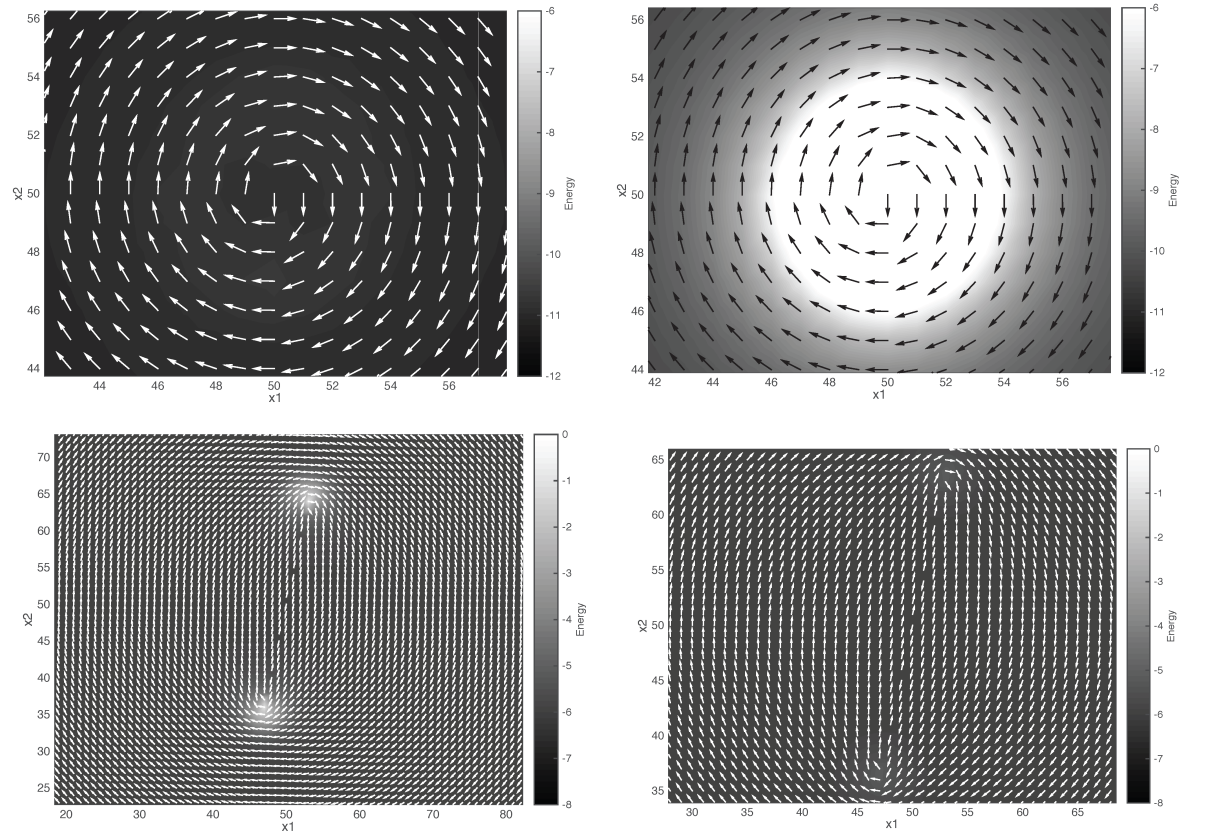

Figure 6: Top row: Energy partitioning into splay (left) and bend (right) in the final configuration for $K_s = 10K_b$, i.e., splay is much more expensive than bending. The defect retains a $+1$ character to minimize splay distortion. Bottom row: Energy partitioning into splay (left) and bend (right) in the final configuration for $K_s = K_b/10$, i.e, bending is much more expensive than splay. The defect dissociates to reduce the bending distortion and compensates with a higher splay distortion.

6 Coalescence of $+\frac{1}{2}$ and $-\frac{1}{2}$ Disclinations

We next use our model to examine the evolution of 2 disclinations of equal-and-opposite $\pm\frac{1}{2}$ topological charge. Two such disclinations will attract each other, causing them to move towards each other and eventually coalesce to form a disclination-free material. Whether these defects move at the same velocity towards each other, and hence coalesce at the midpoint between the initial defect positions, has been an important question. This has been the focus of both experimental and theoretical investigation. A key experiment observing coalescence of *point* defects in nematics shows that there is asymmetry in their motion [CB03]. Closely related situations have been studied numerically and theoretically [SŽ03, TDY02, SŽ02, BS12, GSV02]; while some of these systems are significantly different from the nematics studied here, a key broad finding is the significant influence from hydrodynamic effects. We find here that even without any flow effects, there is asymmetry in defect velocity.

We examine this situation using our simple 1-constant regularized model using $\pm\frac{1}{2}$ disclinations. Fig. 7 shows the initial configuration with two $\pm\frac{1}{2}$ disclinations and the final defect-free configuration. The force between disclinations falls off very rapidly with distance, and hence there is initially little movement. However, as the disclinations begin to come closer, the force increases, thereby further increasing the velocity, and so on. Eventually, the disclinations coalesce and leave behind a disclination-free material. A movie of the coalescence process is part of the supplementary material, and we quantify the approach in Fig. 8. While small, there is an unmistakable difference in the velocities of the positive and negative defects. Given that our 1-constant regularized model contains no complexities such as flow, or even different moduli for bend and splay, it suggests that this asymmetry in disclination velocity has its origin in the asymmetry of the director field; flow further enhances this effect when present [TDY02, SŽ02].

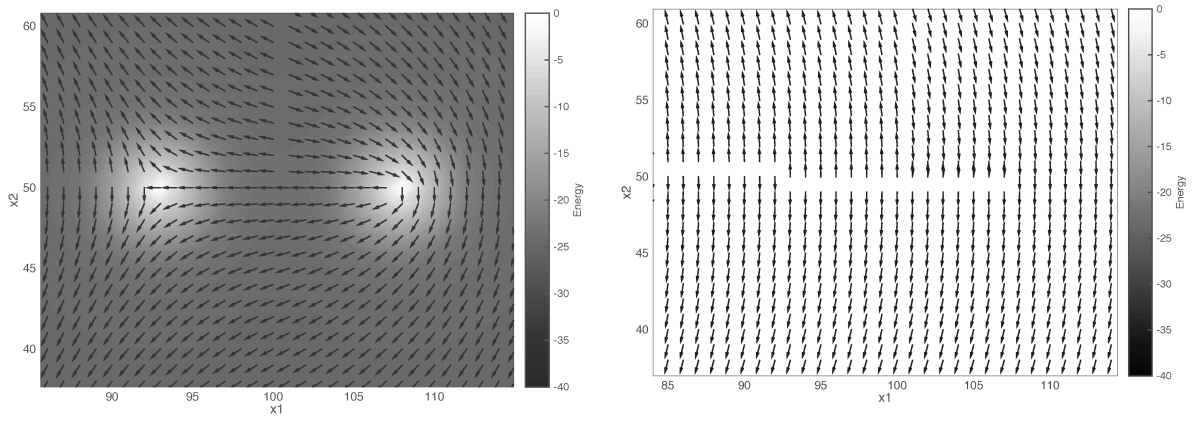

Figure 7: Initial configuration (left) with two $\pm\frac{1}{2}$ defects, and the final defect-free configuration (right).

A priori, there is no reason for equal-and-opposite topological disclinations to move at the same velocity. Disclinations are *not* analogous to electrical point charges which have no internal structure and are there-

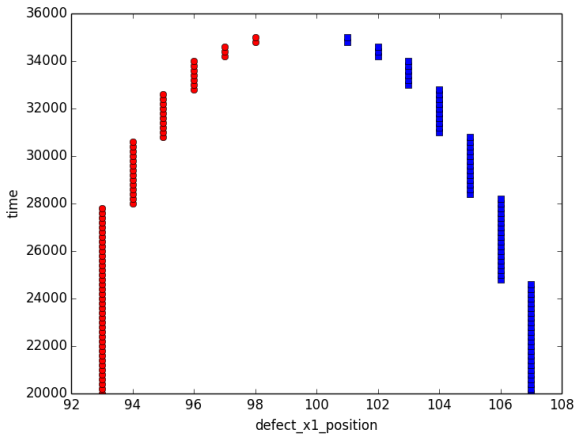

Figure 8: Disclination core positions as a function of time. Red circles are $-\frac{1}{2}$ and blue squares are $+\frac{1}{2}$. The disclination cores are located by finding the mesh point with the highest energy density. The motion appears discontinuous because we only sample over a discrete mesh.
The asymmetry in the motion is immediately obvious. We notice that the $+\frac{1}{2}$ defect has a higher velocity. For instance, the $+\frac{1}{2}$ defect is clearly closer to the midpoint at later times. Also, the $-\frac{1}{2}$ defect stays fixed from $t = 20000$ to $t = 28000$, while the $+\frac{1}{2}$ defect migrates by one grid point in that time.
The velocity increases as the disclinations approach, as is expected [GSV02].

fore perfectly anti-symmetric. Rather, the topological charge is simply one average measure – admittedly an extremely important measure – of the defect structure. The detailed structure of the disclination plays an important role in the dynamics, and even if different disclinations of the same strength have the same force acting on them, the detailed structure is essential in setting the dynamics in response to the force. Returning to the electrical analogy, the net charge is just a particular characterization of a complex charge distribution, but the dynamics of the charge distribution in response to another charge distribution cannot be characterized solely in terms of the net charges of both distributions. Rather, the net charge is simply the lowest-order moment of the distribution. As noted in [GSV02], the configurational (or driving) forces are equal and opposite on defects of equal and opposite sign in the quasi-static setting, arguing from symmetry when the boundaries are sufficiently far away. However, this need not translate to equal and opposite velocities; there is in general no reason for the dissipation (or kinetic) relation associated to the defects of equal and opposite sign to be the same. As [GSV02] further notes, computing the dissipation requires a "non-local" calculation, by which they mean that the director field away from the core is also relevant; this is in accord with the discussion above that the entire director field associated to a defect is relevant and not just the defect charge.

7 Discussion

We present a nonlocal regularized model that exploits integral operators to achieve a generalization of the classical Ericksen-Leslie model for nematics. Near disclinations, the model regularizes defect cores, and as the distortion becomes uniform, it recovers the Ericksen-Leslie model. The use of integral operators – as opposed to differential operators in the classical approach – enables us to model situations in which the disclination field is not continuous. As we describe, the integral operators tend to the differential operators in a physically meaningful way.

Our approach works only with the director field and does not introduce any new quantities, in contrast to [Eri91] for instance. This has the consequent advantage that no new evolution equations need to be introduced, and only the evolution equation for the director is used, which is well-established and based on fundamental principles of angular momentum balance. In this context, we point out the important recent contribution of [BB15] that modifies the standard OZF energy to have subquadratic scaling at large values of the director gradient, thereby obtaining finite energy disclinations with a model based only of the director field; however, this does not introduce a regularizing lengthscale.

Our approach uses in an essential way the important ideas behind peridynamics [Sil00, SL10]. However, the head-tail asymmetry that is essential in describing liquid crystals does not have an analog in peridynamics which is tailored to deformation fields.

This is a preliminary step towards the formulation of this class of models. While we have demonstrated it in the context of nematics, it is readily generalizable to other liquid crystalline material such as smectics. The key issues that we have dealt with here – namely unit vector fields that have discontinuities – are the central challenges in this class of materials. In addition, we have not fit the many material parameters here to specific materials. For instance, the regularization scale δ, the precise form of the kernel C_δ, and the precise angular dependence of K, can all be tailored to capture specific types of physics; for instance, if detailed dynamic behavior is to be predicted. We have also restricted ourselves to 2D for simplicity, but an extension to 3D is conceptually simple. Such an extension would enable the interrogation of more realistic geometries, as well as enable us to examine twist distortions.

Our numerical approximations have used finite differences for simplicity. However, powerful numerical techniques such as discontinuous Galerkin finite elements (DGFEM) can enable the efficiency of adaptive meshing and finite elements to attack much bigger problems and complex geometries with our model. While defect tracking can be enormously expensive, results from [DGLZ12, CG11] suggest that DGFEM offers an efficient approach: it is a conforming approximation for peridynamics, and the results appear not very sensitive to the errors in tracking the defect.

Our numerical calculation of the coalesence of two disclinations of equal and opposite sign shows an interesting asymmetry that is not predicted by other approaches. While we have focused on the simplest possible setting to isolate the effect from other complexities, a systematic study of various configurations is a potential direction for future research.

Our numerical calculation of the splitting of a $+2$ disclination shows qualitative differences from predictions by the Q-tensor theory. It is not clear which is closer to reality in terms of experimental observation. A very significant challenge in doing this experiment is that $+2$ defects are unstable so it is not clear how to set up an initial condition with such a configuration. Molecular dynamics may provide answers, but the issue of timescales is a significant hurdle.

Acknowledgments

We thank John Ball, Chuck Gartland, Nigel Mottram, and Noel Walkington for valuable discussions and pointers to the literature. We acknowledge support from: (1) NSF Mechanics of Materials and Structures (CAREER 1150002 and 1635407), NSF Manufacturing Machines and Equipment (1635435), ARO Numerical Analysis (YI W911NF-12-1-0156 and W911NF-17-1-0084), and ONR Applied and Computational Analysis (N00014-14-1-0715 and N00014-18-1-2528); (2) the Department of Mathematics at the University of Bath through the Parkin Visiting Professorship; (3) the Air Force Summer Faculty Fellowship Program (4) an appointment to the National Energy Technology Laboratory Faculty Research Participation Program sponsored by the U.S. Department of Energy and administered by the Oak Ridge Institute for Science and Education; and (5) the National Science Foundation through XSEDE resources provided by Pittsburgh Supercomputing Center.

A An Alternative Approach to the Energetics of Bend and Splay

The classical model of nematic liquid crystals uses the kinematic quantities $\nabla \cdot \boldsymbol{n}$, $\boldsymbol{n} \cdot \nabla \times \boldsymbol{n}$, and $\boldsymbol{n} \times \nabla \times \boldsymbol{n}$ to measure splay, twist, and bend respectively. The energetics of these deformation modes are simply given by $(\nabla \cdot \boldsymbol{n})^2$, $(\boldsymbol{n} \cdot \nabla \times \boldsymbol{n})^2$, and $(\boldsymbol{n} \times \nabla \times \boldsymbol{n})^2$, with appropriate moduli for each mode. We briefly consider here an alternative approach to nonlocal analogs of these quantities.

The 1-constant energy in (3.3) can be considered the nonlocal analog of $\nabla \boldsymbol{n} : \nabla \boldsymbol{n}$, i.e. the double contraction of the gradient of $\boldsymbol{n}$. In index notation:

$$n_{i,j} n_{i,j} \sim \int_{\hat{\boldsymbol{x}} \in \Omega} \left(\hat{n}_i - n_i\right) \left(\hat{x}_j - x_j\right) \left(\hat{n}_i - n_i\right) \left(\hat{x}_j - x_j\right) \, dV_{\hat{\boldsymbol{x}}} \tag{A.1}$$

where normalizing factors have been neglected for clarity.

Extending this reasoning, we can write the nonlocal analogs of splay, twist, and bend as follows:

$$n_{i,i}n_{j,j} \sim \int_{\hat{\boldsymbol{x}}\in\Omega} (\hat{n}_i - n_i)\,(\hat{x}_i - x_i)\,(\hat{n}_j - n_j)\,(\hat{x}_j - x_j)\; dV_{\hat{\boldsymbol{x}}} \tag{A.2}$$

$$n_i\epsilon_{ijk}n_{j,k}n_l\epsilon_{lmn}n_{m,n} \sim \epsilon_{ijk}\epsilon_{lmn}\int_{\hat{\boldsymbol{x}}\in\Omega} n_i n_l\,(\hat{n}_j - n_j)\,(\hat{x}_k - x_k)\,(\hat{n}_m - n_m)\,(\hat{x}_m - x_m)\; dV_{\hat{\boldsymbol{x}}} \tag{A.3}$$

$$\epsilon_{abk}n_b\epsilon_{kji}n_{j,i}\epsilon_{apq}n_p\epsilon_{qrs}n_{r,s} \sim \epsilon_{abk}\epsilon_{kji}\epsilon_{apq}\epsilon_{qrs}\int_{\hat{\boldsymbol{x}}\in\Omega} n_b n_p\,(\hat{n}_j - n_j)\,(\hat{x}_i - x_i)\,(\hat{n}_r - n_r)\,(\hat{x}_s - x_s)\; dV_{\hat{\boldsymbol{x}}} \tag{A.4}$$

References

[A$^+$93] PJ Andrew et al. Monte carlo investigations of a gayâĂŤberne liquid crystal. *Journal of the Chemical Society, Faraday Transactions*, 89(22):4069–4078, 1993.

[AD14] Amit Acharya and Kaushik Dayal. Continuum mechanics of line defects in liquid crystals and liquid crystal elastomers. *Quarterly of Applied Mathematics*, 72(1):33–64, 2014.

[AKST14] François Alouges, Evaggelos Kritsikis, Jutta Steiner, and Jean-Christophe Toussaint. A convergent and precise finite element scheme for landau–lifschitz–gilbert equation. *Numerische Mathematik*, 128(3):407–430, 2014.

[BB15] John M Ball and SJ Bedford. Discontinuous order parameters in liquid crystal theories. *Molecular Crystals and Liquid Crystals*, 612(1):1–23, 2015.

[BGJRV03] Fulvio Bisi, Eugene C Gartland Jr, Riccardo Rosso, and Epifanio G Virga. Order reconstruction in frustrated nematic twist cells. *Physical Review E*, 68(2):021707, 2003.

[BKŽ98] Zlatko Bradač, Samo Kralj, and Slobodan Žumer. Molecular dynamics study of nematic structures confined to a cylindrical cavity. *Physical Review E*, 58(6):7447, 1998.

[BPP12] Patricia Bauman, Jinhae Park, and Daniel Phillips. Analysis of nematic liquid crystals with disclination lines. *Arch. Ration. Mech. Anal.*, 205(3):795–826, 2012.

[BS12] Paolo Biscari and Timothy J Sluckin. A perturbative approach to the backflow dynamics of nematic defects. *European Journal of Applied Mathematics*, 23(01):181–200, 2012.

[BVD04] Fulvio Bisi, Epifanio G Virga, and Georges E Durand. Nanomechanics of order reconstruction in nematic liquid crystals. *Physical Review E*, 70(4):042701, 2004.

[CB03] PE Cladis and Helmut R Brand. Hedgehog–antihedgehog pair annihilation to a static soliton. *Physica A: Statistical Mechanics and its Applications*, 326(3):322–332, 2003.

[CG11] Xi Chen and Max Gunzburger. Continuous and discontinuous finite element methods for a peridynamics model of mechanics. *Computer Methods in Applied Mechanics and Engineering*, 200(9):1237–1250, 2011.

[CL00] Paul M Chaikin and Tom C Lubensky. *Principles of condensed matter physics*, volume 1. Cambridge Univ Press, 2000.

[CLB+09] Giovanni Carbone, Giuseppe Lombardo, Riccardo Barberi, Igor Muševič, and Uroš Tkalec. Mechanically induced biaxial transition in a nanoconfined nematic liquid crystal with a topological defect. *Physical review letters*, 103(16):167801, 2009.

[DB06] Kaushik Dayal and Kaushik Bhattacharya. Kinetics of phase transformations in the peridynamic formulation of continuum mechanics. *Journal of the Mechanics and Physics of Solids*, 54(9):1811–1842, 2006.

[DGLZ12] Qiang Du, Max Gunzburger, Richard B Lehoucq, and Kun Zhou. Analysis and approximation of nonlocal diffusion problems with volume constraints. *SIAM review*, 54(4):667–696, 2012.

[dP95] P deGennes and J Prost. *The physics of liquid crystals*. Number 83. Oxford university press, 1995.

[Eri91] Jerald L Ericksen. Liquid crystals with variable degree of orientation. *Archive for Rational Mechanics and Analysis*, 113(2):97–120, 1991.

[GSV02] Eugene C Gartland, Jr, André M Sonnet, and Epifanio G Virga. Elastic forces on nematic point defects. *Continuum Mechanics and Thermodynamics*, 14(3):307–319, 2002.

[HDCK12] M Holovko, D Di Caprio, and I Kravtsiv. Maier-saupe nematogenic fluid: field theoretical approach. *arXiv preprint arXiv:1202.4548*, 2012.

[KL07] Maurice Kléman and Oleg D Lavrentovich. *Soft matter physics: an introduction*. Springer Science & Business Media, 2007.

[KLGCC08] D Harley Klein, L Gary Leal, Carlos J García-Cervera, and Hector D Ceniceros. Three-dimensional shear-driven dynamics of polydomain textures and disclination loops in liquid crystalline polymers. *Journal of Rheology (1978-present)*, 52(3):837–863, 2008.

[LL72] Paul A Lebwohl and Gordon Lasher. Nematic-liquid-crystal orderâĂŤa monte carlo calculation. *Physical Review A*, 6(1):426, 1972.

[MHML05] Dmitri Miroshnychenko, NA Hill, NJ Mottram, and JE Lydon. Evolution from a+ 2 defect to+ 1/2 defects in a cylindrical geometry. *Molecular Crystals and Liquid Crystals*, 437(1):251–1495, 2005.

[MN14] Nigel J Mottram and Christopher JP Newton. Introduction to q-tensor theory. *arXiv preprint arXiv:1409.3542*, 2014.

[MPR14] Bryce S Murray, Robert A Pelcovits, and Charles Rosenblatt. Creating arbitrary arrays of two-dimensional topological defects. *Physical Review E*, 90(5):052501, 2014.

[PAD15] Hossein Pourmatin, Amit Acharya, and Kaushik Dayal. A fundamental improvement to ericksen-leslie kinematics. *Quarterly of Applied Mathematics*, 73(3):435–466, 2015.

[PB94] Michael Plischke and Birger Bergersen. *Equilibrium statistical physics*. World Scientific Publishing Co Inc, 1994.

[PMGK94] P Palffy-Muhoray, EC Gartland, and JR Kelly. A new configurational transition in inhomogeneous nematics. *Liquid Crystals*, 16(4):713–718, 1994.

[PP01] NV Priezjev and Robert A Pelcovits. Cluster monte carlo simulations of the nematic-isotropic transition. *Physical Review E*, 63(6):062702, 2001.

[Sil00] Stewart A Silling. Reformulation of elasticity theory for discontinuities and long-range forces. *Journal of the Mechanics and Physics of Solids*, 48(1):175–209, 2000.

[SL10] SA Silling and RB Lehoucq. Peridynamic theory of solid mechanics. *Advances in Applied Mechanics*, 44(1):73–166, 2010.

[SMV04] AM Sonnet, PL Maffettone, and EG Virga. Continuum theory for nematic liquid crystals with tensorial order. *Journal of non-newtonian fluid mechanics*, 119(1):51–59, 2004.

[Ste04] Iain W Stewart. *The static and dynamic continuum theory of liquid crystals: a mathematical introduction*. Crc Press, 2004.

[SŽ02] Daniel Svenšek and Slobodan Žumer. Hydrodynamics of pair-annihilating disclination lines in nematic liquid crystals. *Physical Review E*, 66(2):021712, 2002.

[SŽ03] D Svenšek and S Žumer. Hydrodynamics of pair-annihilating disclinations in sm-c films. *Physical review letters*, 90(15):155501, 2003.

[TDY02] Géza Tóth, Colin Denniston, and Julia M Yeomans. Hydrodynamics of topological defects in nematic liquid crystals. *Physical review letters*, 88(10):105504, 2002.

[YFMW09] Xiaofeng Yang, M Gregory Forest, William Mullins, and Qi Wang. Dynamic defect morphology and hydrodynamics of sheared nematic polymers in two space dimensions. *Journal of Rheology (1978-present)*, 53(3):589–615, 2009.

[YR02] Jun Yan and AD Rey. Theory and simulation of texture formation in mesophase carbon fibers. *Carbon*, 40(14):2647–2660, 2002.

[ZZA$^+$] Chiqun Zhang, Xiaohan Zhang, Amit Acharya, Dmitry Golovaty, and Noel Walkington. A non-traditional view on the modeling of nematic disclination dynamics. *preprint*.